

Universidad de Granada

GRADO EN FÍSICA

KURAMOTO'S MODEL AND  
SYNCHRONISATION.

*Physics of complex systems*



UNIVERSIDAD  
DE GRANADA

Jerónimo Aragón, Rafael  
Liñán Contreras, Juan

20/06/2024

**Abstract**

In this project, a full analytical and simulation study about the Kuramoto's Model is done. Comparison between both approaches to the problem and observation of the described phenomena are the main purpose of it. It will be also done a comparison with different distribution of intrinsic velocities and a study of the model in 2 dimensions.

**Contents**

|          |  |           |
|----------|--|-----------|
| <b>1</b> | <b>Introduction and interest cases.</b>  | <b>2</b>  |
| <b>2</b> | <b>Mean field analysis and obtention of critical points.</b>   | <b>2</b>  |
| 2.1      | Summary of results . . . . .   | 4         |
| <b>3</b> | <b>Numerical simulation of the theoretical model.</b>  | <b>5</b>  |
| 3.1      | Model's Simulation. . . . .  | 5         |
| 3.2      | Variation of $r$ with $K$ . . . . .  | 7         |
| 3.2.1    | Alternative obtaining of $r$ . . . . .   | 7         |
| 3.2.2    | Comparison of the data obtained ( $r$ ) with the analytical value. . . . .                                 | 8         |
| <b>4</b> | <b>Differences between unimodal and bimodal distributions</b>  | <b>11</b> |
| <b>5</b> | <b>The Kuramoto's Model in two dimensions. Appearance of patterns associated with Turing instabilities</b> | <b>13</b> |
| <b>6</b> | <b>Renormalization Group Analysis of Kuramoto's Model</b>  | <b>17</b> |
| <b>7</b> | <b>Conclusions</b>   | <b>18</b> |
| <b>8</b> | <b>Appendix</b>  | <b>19</b> |
| 8.1      | Normalization conditions for the mean field analysis section. . . . .                                      | 19        |
| 8.2      | Links to the videos, data generated and used for each case and the codes. . . . .                          | 19        |
| 8.3      | Errors determination . . . . .   | 19        |

## 1 Introduction and interest cases.

The second law of thermodynamics declares that everything in the universe tends to disorder, and as it is well known, in complex systems, chaos is the rule followed. So, it may not be inappropriate to think that synchronization in the universe is something quite rare. But, just one look at the nature is sufficient to observe plenty examples of its spontaneous appearance: The synchronization of the metronomes placed in the same surface, the simultaneous flashes of fireflies, the pendulum clocks that after a certain period go on time (phase opposition) having been initially placed in different conditions,... What puts these things in order in spite of worlds tendency to disorder? Even though this phenomena has been qualitatively described by physicist since Huygens's time, it was not until a few decades ago that a consistent model for synchronization has been released.

## 2 Mean field analysis and obtention of critical points.

First exposed by Kuramoto in 1984, the interest of this canonical mathematical model relies in its capacity of describe the spontaneous synchronization that arise when a great number of coupled oscillator interact between each other. The type of interaction and the grade of coupling among the oscillators will define the phenomena.

In the case analyzed in [1] (the simplest)  $N$  oscillators will be considered, each of them running at its own frequency  $\omega_i$  and been connected to the others through an equal coupling constant ( $K$ ). The interaction adjusts sinusoidal to the phase difference between each pair of oscillators, that is, between the subject in question and each of the others. Taking that idea into the math, the following system of  $N$  equations arise:

$$\frac{d\theta_i}{dt} = \omega_i + \frac{k}{N} \sum_{j=1}^N \sin(\theta_j - \theta_i) \quad (2.1)$$

So the system is composed by  $N$  oscillators  $\theta_i(t)$  which are trying to run at its own frequency whereas the coupling between them tries to synchronize the whole pack. So the first question that comes to the mind is, how different are these frequencies?

In all the analysis that is about to be done the intrinsic frequencies will be obeying a certain unimodal probability distribution called Lorentzian (or Cauchy, it depends on the source) distribution:

$$g(\omega) = \mathcal{L}(\omega; 0, \gamma) = \frac{1}{\pi} \left[ \frac{\gamma}{\omega^2 + \gamma^2} \right]$$

which is centered on  $\omega_0 = 0$ . Knowing this, it is reasonable to presuppose that the coherence of the system would depend directly on how strong the coupling is. While it is weak, no apparent synchronization will arise and the pack will evolve incoherently, but there will be a point, a certain limit, from which the collection synchronization surely will emerge.

The first objective of this project is to find it. The following development is mainly based in what can be found in [1]. Here, synchronization is conveniently measured by an order parameter.

Taking  $K = \frac{k}{N} > 0$  in 2.1 and rewritten it in terms of a complex value order parameter:

$$re^{i\psi} = \frac{1}{N} \sum_{j=1}^N e^{i\theta_j} \quad (2.2)$$

$r(t) \in [0,1]$  and it measures the coherence of oscillators population, while  $\psi(t)$  is the average phase of the system. With this definition the equation 2.1 becomes:

$$\dot{\theta}_i = \omega_i + Kr \sin(\psi - \theta_i) \quad (2.3)$$

and it is evident that each oscillator adjusts to the phase average with a strength determined by  $Kr$ . It is convenient (in order to develop what is next) to take in count the next equivalence for equation 2.2

$$re^{i\psi} = \int_{-\pi}^{\pi} e^{i\theta} \left( \frac{1}{N} \sum_{j=1}^N \delta(\theta - \theta_j) \right) d\theta$$

As  $N$  tends to the limit of infinite oscillators ( $N \rightarrow \infty$ ) they will be distributed with a new probability density function  $\rho(\theta, \omega, t)$  (probability of finding one oscillator with a phase  $\theta$ , a frequency  $\omega$ , at a time  $t$ ) so that equation 2.2 becomes now:

$$re^{i\psi} = \int_{-\pi}^{\pi} \int_{-\infty}^{\infty} e^{i\theta} \rho(\theta, \omega, t) g(\omega) d\theta d\omega \quad (2.4)$$

From the previous equations some conclusion can already be obtained:

- When  $K \rightarrow 0$  : Equation 2.3 implies  $\dot{\theta}_i = \omega_i t + \omega(0)$  so each oscillator runs at its natural frequency. That would mean that  $r=0$  in this case. It is easy to prove it, just putting  $\theta = \omega t$  in equation 2.4 and appealing to the Riemann-Lebesgue lemma [2] it is clear that  $r=0$  as  $t \rightarrow \infty$
- On the other hand, as each oscillator is coupled to the average phase depending on  $Kr$ , if  $K \rightarrow \infty$  :  $\theta_i \approx \psi$  and replacing it in 2.4:

$$re^{i\psi} = e^{i\psi} \int_{-\pi}^{\pi} \int_{-\infty}^{\infty} \rho(\theta, \omega, t) g(\omega) d\theta d\omega \rightarrow r = 1$$

(In which the Normalization conditions ( section 8.1) for both probability distributions has been used)

So, the problem is solved for weak and strong coupling. What happens for intermediate cases?  $0 < K < \infty$ . Let's keep bringing new equations that can be helpful.

As a density function has been introduced, it must follow a continuity equation, that would be:

$$\frac{\partial \rho}{\partial t} + \frac{\partial}{\partial \theta} (\rho [\omega + Kr \sin(\psi - \theta)]) = 0 \quad (2.5)$$

Under what conditions could  $r$  arise? Seeing 2.3 it is obvious that a random oscillator will become stably locked at an angle such that  $Kr \sin(\theta - \psi) = \omega$  with the condition of  $-\frac{\pi}{2} \leq (\theta - \psi) \leq \frac{\pi}{2}$ .

Oscillators with frequencies  $|\omega| > kr$  cannot be locked, they will always evolve out of synchrony. Their stationary density obeys  $\frac{\partial \rho}{\partial t} = 0 \rightarrow \rho \dot{\theta} = C(\omega)$ ; So the density function will be:

$$\rho = \frac{C(\omega)}{\dot{\theta}} = \frac{C(\omega)}{|\omega - Kr \sin(\theta - \psi)|}$$

## 2.1 Summary of results 2 MEAN FIELD ANALYSIS AND OBTENTION OF CRITICAL POINTS.

and taking in count the normalization condition it is possible to find  $C(\omega)$ , but in this case is has not great interest. To sum up all this in an unique cases equation:

$$\rho = \begin{cases} \delta[\theta - \psi - \arcsin(\frac{\omega}{Kr})] & \text{if } |\omega| < Kr \\ \frac{C(\omega)}{|\omega - Kr\sin(\theta - \psi)|} & \text{elsewhere (not locked)} \end{cases} \quad (2.6)$$

Now, replacing what has been found in the equation 2.4, a expression for r can be obtained:

$$r = \int_{-\frac{\pi}{2}}^{\frac{\pi}{2}} \int_{-\infty}^{\infty} e^{i(\theta-\psi)} \delta[\theta - \psi - \arcsen(\frac{\omega}{Kr})] g(\omega) d\theta d\omega \\ + \int_{-\pi}^{\pi} \int_{|\omega| > Kr} e^{i(\theta-\psi)} \frac{C(\omega)g(\omega)}{|\omega - Kr\sin(\theta - \psi)|} d\theta d\omega$$

The second double integral is zero due to symmetries relations and the first can be expressed as:

$$r = \int_{|\omega| < Kr} \cos(\arcsen(\frac{\omega}{Kr})) g(\omega) d\omega \rightarrow \\ r = \int_{-\frac{\pi}{2}}^{\frac{\pi}{2}} \cos^2(\theta) g(Kr\sin(\theta)) Krd\theta \rightarrow \\ 1 = K \int_{-\frac{\pi}{2}}^{\frac{\pi}{2}} \cos^2(\theta) g(Kr\sin(\theta)) d\theta \quad (2.7)$$

From this, the value of the critical point  $K_c$  can be calculated as the limit for r=0:

$$1 = K_c \int_{-\frac{\pi}{2}}^{\frac{\pi}{2}} \cos^2(\theta) g(0) d\theta \rightarrow K_c = \frac{2}{\pi g(0)} \quad (2.8)$$

And reminding that in this case  $g(\omega) = \frac{1}{\pi} [\frac{\gamma}{\omega^2 + \gamma^2}]$  then  $g(0) = \frac{1}{\pi\gamma}$  and replacing back into the equation, the more important results of the analytical part are obtained:

$$K_c = 2\gamma \quad (2.9)$$

$$r = \sqrt{1 - \frac{K_c}{K}} \quad (2.10)$$

### 2.1 Summary of results

A brief summary with all the analytical conclusions would clarify everything before the numerical simulation is carried out. So mainly three situations can be studied.

1. For  $K < K_c = 2\gamma$  : There is no synchronization at all, so r=0 (here, equation 2.10 does not apply as it makes sense for  $K \geq K_c$ ) and the oscillators evolve without being locked at any time.
2. For  $K_c \leq K < \infty$  : The system is partially synchronized as some oscillators (those which  $|\omega| < Kr$ ) run coherently while others do not locked. As K increases, the previous condition is easier to comply and r also grows following equation 2.10.
3. For  $K \rightarrow \infty$  : r=1 and the whole system runs coherently.

### 3 Numerical simulation of the theoretical model.

In the previous section, the analytical development has been researched and understood with the purpose of knowing what to expect in the simulations and check that good results have been obtained. In this one, the computer takes the main place, as the model has been simulated with a code in C++ which runs with all its variables. In the next subsections different parts of the simulation are exposed and explained.

#### 3.1 Model's Simulation.

Some settings (initial conditions) that are necessary to know and that all the results exposed here fulfill:

- The initial angle  $\theta_0$  of each oscillator is randomized in the program.
- The number of oscillators are  $N=100$
- Time steps below 0.01
- For the lorentzian distribution of intrinsic velocities, its properties are:  $\omega_0 = 0$  and  $\gamma = 1$

From here, the code is able to represent the angle depending on time for all the oscillator in a video, from which some images (different in time) has been taken. This has been made for several values of K.

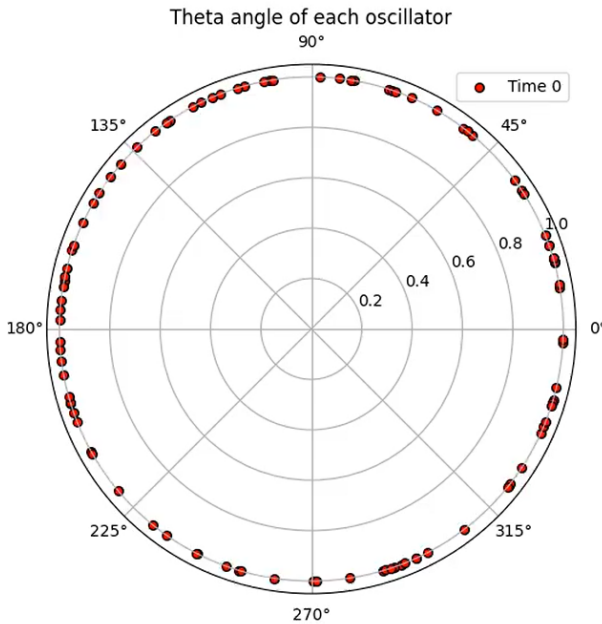
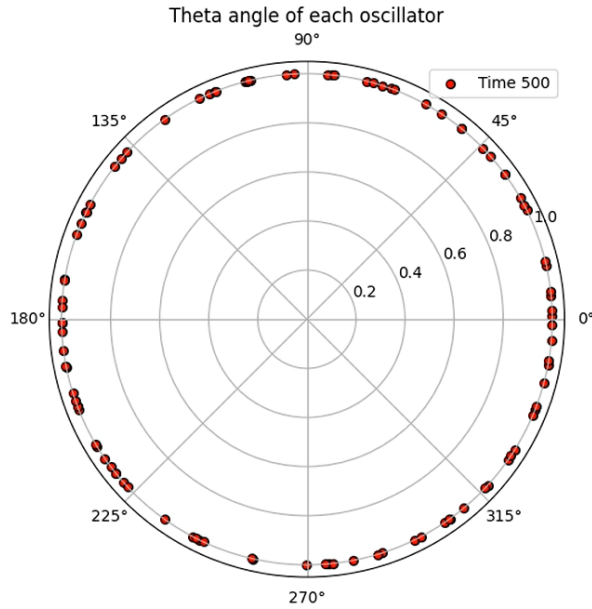
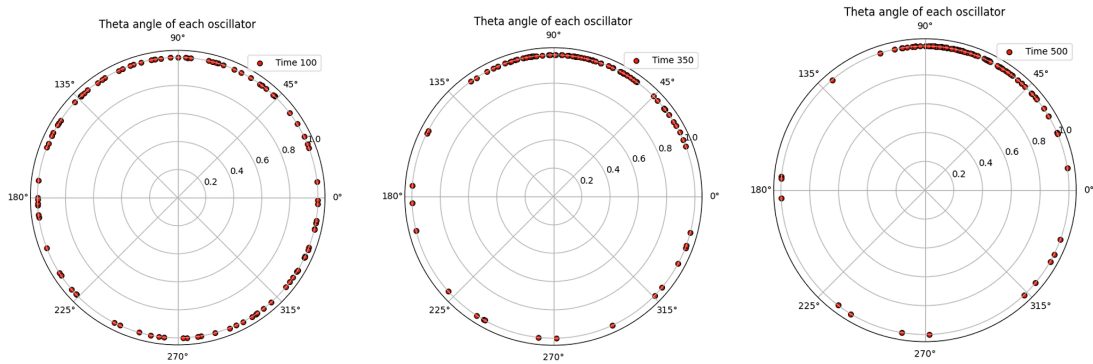
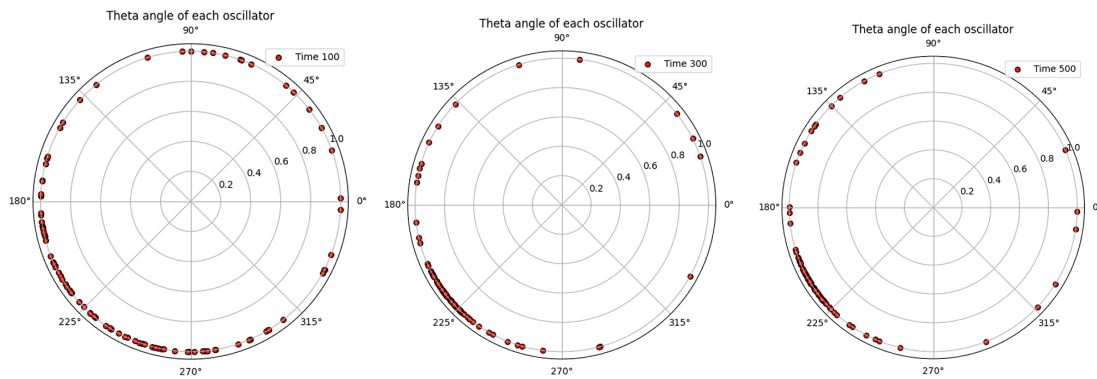


Figure 1: Angle of each particle at time  $t=0$  for  $K$  near 0

Figure 1 shows how the initial angle for the different particles is random. For every other case, with different K, it is not very different, there are an approximate homogeneous distribution in all the initial state. To avoid repetition, that is the only figure that will show angles at time  $t=0$ .

Figure 2: Angle of each particle at time  $t=500$  for  $K=0$ Figure 3: Angle of each oscillator at times  $t=100$ ,  $t=350$  and  $t=500$ , from left to right, for  $K=5$ Figure 4: Angle of each oscillator at times  $t=100$ ,  $t=300$  and  $t=500$ , from left to right, for  $K=10$

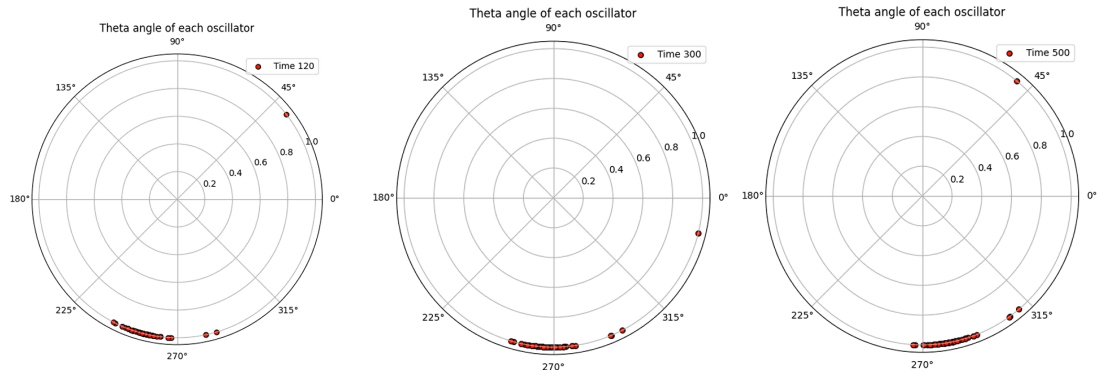


Figure 5: Angle of each oscillator at times  $t=120$ ,  $t=300$  and  $t=500$ , from left to right, for  $K=20$

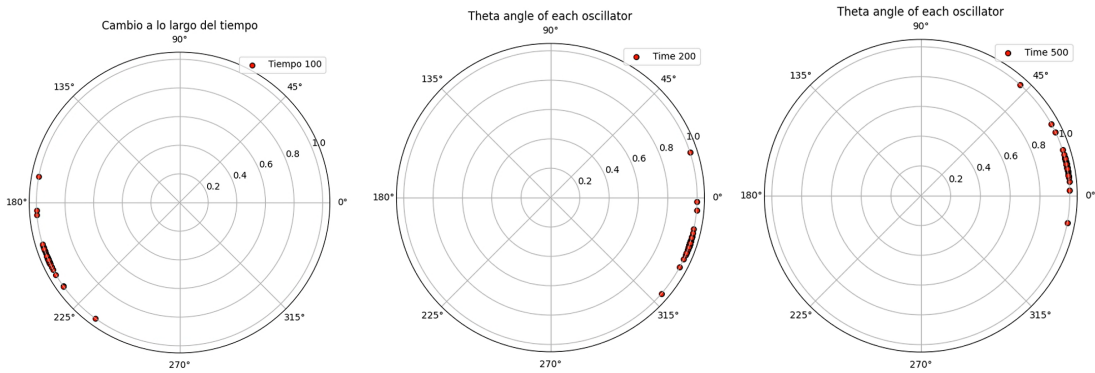


Figure 6: Angle of each oscillator at times  $t=120$ ,  $t=300$  and  $t=500$ , from left to right, for  $K=100$

It is clear that the behaviour is the one expected. Figure 2 reveal how for a weak coupling there is no synchronization even after a considerable quantity of time has past. On the other hand, figures 3 and 4 shows perfectly how the partial synchronization is working, keeping locked the particles which  $|\omega| < Kr$ . It can be seen also that the time which takes the system to be the most possible coupled (particles with  $|\omega| < Kr$  coupled) decreases with  $K$ . Finally, figure 5 shows all oscillators synchronized but a very intrinsically fast one and figure 6 shows how all the particles are synchronized and evolving coherently, even if they have a phase difference, as none of the oscillators have enough intrinsic velocity to overcome coupling. This is visually consistent with what has been explained in the analytical section.

In order to have a mathematical comparison of the values obtained with respect to the values expected theoretically by the equation 2.10, it was necessary to measure  $r$  with the program. To do this, a development had to be carried out from equation 2.2, to express 2.10 in function of the data that the code possesses.

## 3.2 Variation of $r$ with $K$

### 3.2.1 Alternative obtaining of $r$

Lets see what can be done with the dependence of  $r$  and the angles: From equation 2.2 it is immediate that:

$$r = \frac{1}{N} \frac{\sum_j^N (\cos(\theta_j) + i\sin(\theta_j))}{\cos(\psi_j) + i\sin(\psi_j)} = \frac{1}{N} \frac{\text{Cos}(\theta_j) + i\text{Sen}(\theta_j)}{\cos(\psi_j) + i\sin(\psi_j)}$$

$$r = \frac{1}{N} \operatorname{Re} \left[ \frac{\operatorname{Cos}(\theta_j) + i \operatorname{Sen}(\theta_j)}{\operatorname{cos}(\psi_j) + i \operatorname{sen}(\psi_j)} \right] = \frac{1}{N} \operatorname{Re} [(\operatorname{Cos}(\theta_j) + i \operatorname{Sen}(\theta_j))(\operatorname{cos}(\psi_j) - i \operatorname{sen}(\psi_j))]$$

Making the proper counts and simplifying:

$$r = \frac{1}{N} \left( \sum_j^N (\operatorname{cos}(\theta_j)) \operatorname{cos}(\psi_j) + \sum_j^N (\operatorname{sen}(\theta_j)) \operatorname{sen}(\psi_j) \right)$$

With this alternative way (obtainable by the computer values) of having the value of  $r$ , comparison with the theoretical one calculated by equation 2.10 is possible.

### 3.2.2 Comparison of the data obtained ( $r$ ) with the analytical value.

It could seem to be easy just to compare the values of  $r$  obtained by these two different ways, but a problem emerge.

As it is seen in figures 7,8, it is very hard to notice differences of  $r$  when  $K$  is high, and the deviation with respect with the theoretical value is hard to be calculated as the progression is not linear. Because of that, it is very hard to contrast with the analytical value.

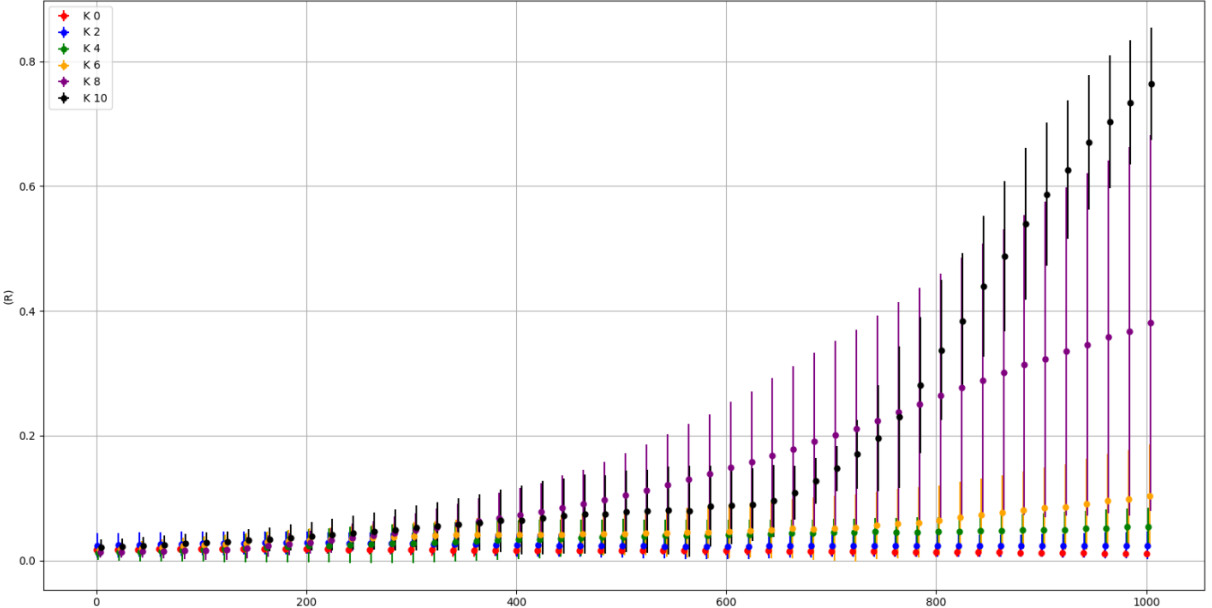
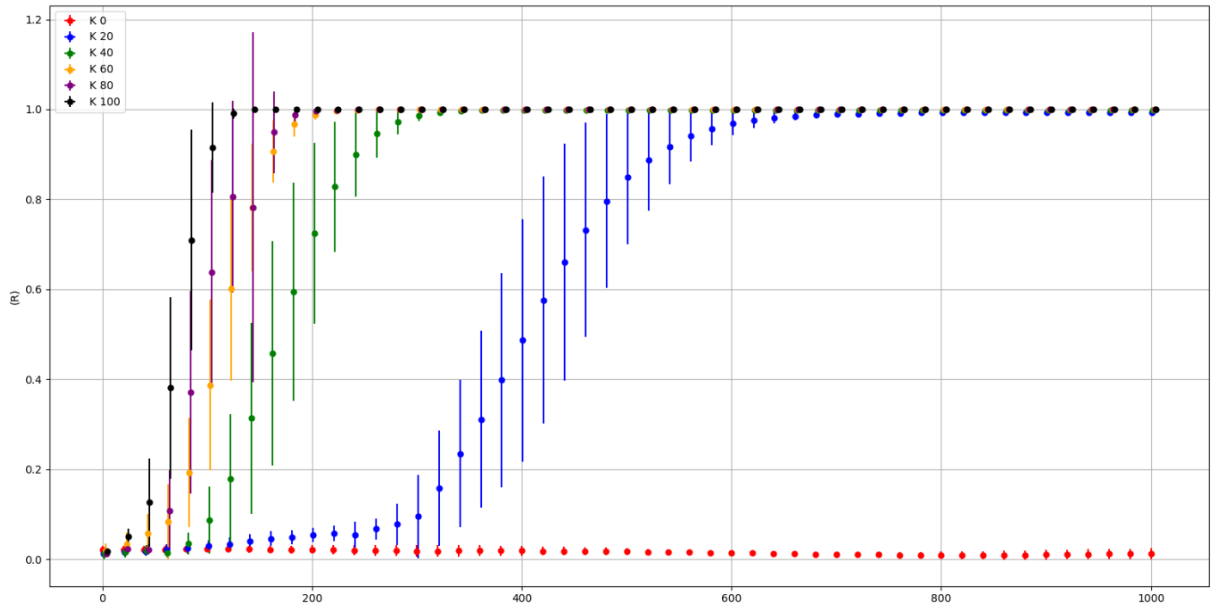


Figure 7:  $R$  as a function  $T$  for low  $K$ 's

Figure 8:  $R$  as a function  $T$  for high  $K$ 's

In order to avoid the problem, the equation 2.10 is manipulated, one reaching:

$$\frac{K}{K_c} = \frac{1}{1 - r^2}$$

And from here a direct comparison method arise. Let  $y = mK$ , with  $m = \frac{1}{K_c}$  and  $y = \frac{1}{1 - r^2}$ . The theoretical value of the slope  $m$  would be  $m = 0.5$  due to the fact that in the simulations  $\gamma = 1 \rightarrow K_c = 2\gamma = 2$ . If  $\frac{1}{1 - r^2}$  points are represented for different  $K$ , which implies different  $r$  ( taking the computational value of it, that has been obtained by the previous method), and adjust them to a linear regression as they should be equal, the slope  $m$  of that adjust should be 0.5.

Figures 9 and 10 show the linear regression realized for  $N=100$  and  $N=1000$  respectively, with the theoretical slope and the regression slope which result in them.

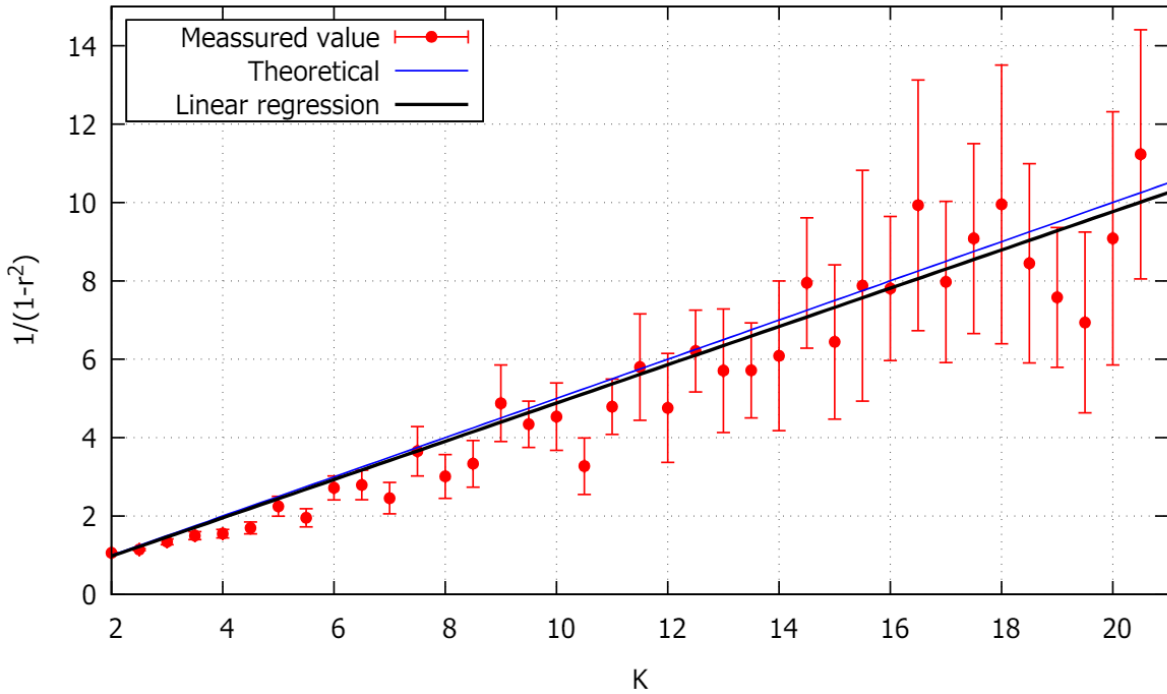


Figure 9: Linear regression of the obtained data and comparison with the theoretical one with  $N=100$

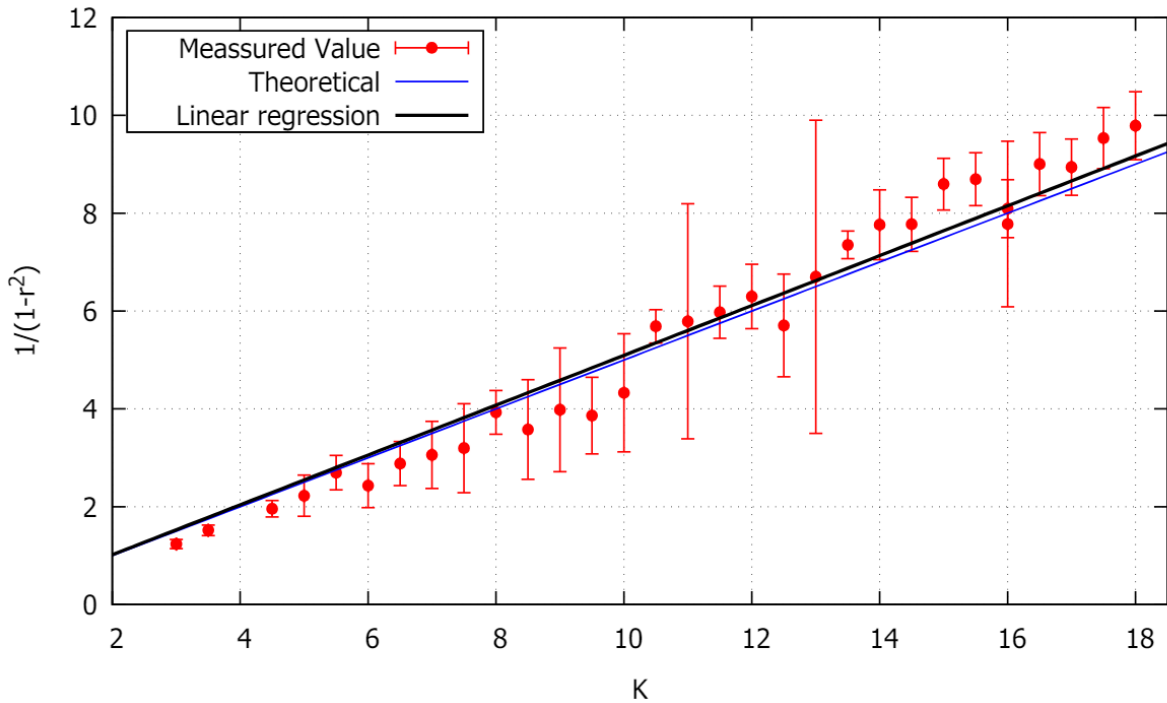


Figure 10: Linear regression of the obtained data and comparison with the theoretical one with  $N=1000$

|           | Slope (m)           | Relative error ( $\epsilon$ ) | $\chi^2$ | $\chi_{th}^2$ (95%) |
|-----------|---------------------|-------------------------------|----------|---------------------|
| Figure 9  | $0.4883 \pm 0.0087$ | 2.34%                         | 115.52   | 52.19               |
| Figure 10 | $0.5093 \pm 0.0095$ | 1.87%                         | 41.15    | 43.77               |

Table 1: Results of Figures 9 (37 degrees of freedom) and 10 (30 DOF).

In table 1 it is visible why it was needed to do the linear regression for  $N=1000$  even though for  $N=100$  the slope had a value very close to the theoretical (2.34% of relative error). The  $\chi^2$  was bigger than  $\chi_{th}^2$  and, by that, a better regression was necessary.  $N=1000$  had less points because, as every oscillator is connected to every other one, computational time rocketed with  $N$  passing from  $N=100$  to  $N=1000$ . However, with  $N=1000$  the results improved a bit and  $\chi^2$  was reduced greatly to achieve it to be less than the theoretical.

## 4 Differences between unimodal and bimodal distributions

For a bimodal distribution there are more possible outcomes than for a Lorentzian (unimodal) distribution of intrinsic velocities, where there is only: no cohesion, partial cohesion in 1 group, total cohesion for very high  $K$ . In bimodal distribution the outcome varies greatly depending on the initial conditions. The following cases gives some outcomes that can happen with certain initial conditions. It has to be taken into account that some conditions repeats from the case of the unimodal, as, random initial angles,  $N=100$ , steps under 0.01 and  $\gamma=1$ .

In certain cases, when the intrinsic velocity of one group is much higher in absolute value than the other, it can provoke the group of slow oscillators to never form because of the influence of the group of oscillators with high intrinsic velocities. This case is, for example, which happens in figure 11.

If  $K$  is sufficiently high the second group can also be formed, existing 2 clusters, as in figure 12.

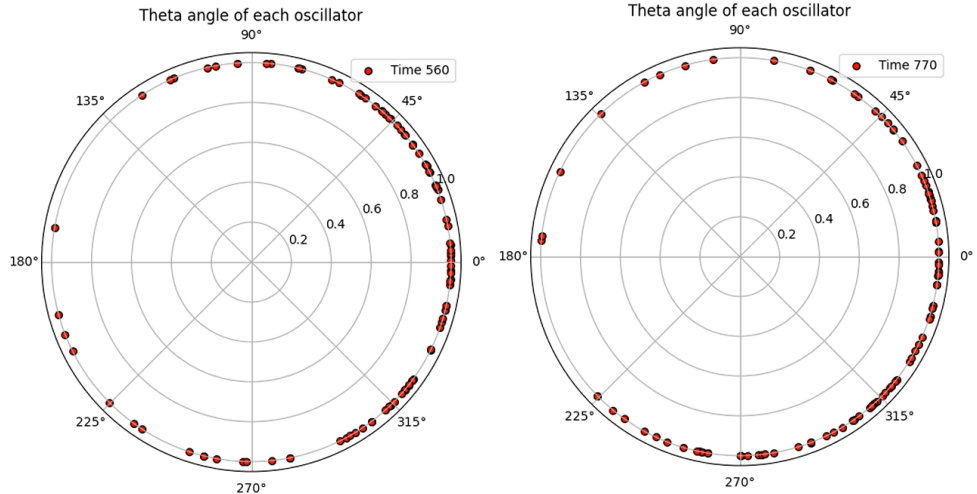


Figure 11: Bimodal distribution. Angle of each oscillator at time  $t=560$  and  $t=770$  for  $K=4$ . Here two clusters are formed. One with the average intrinsic velocity of -1 and the other with +6. The cluster with low intrinsic velocity is weak and even is broken sometimes when the oscillators of the fast cluster go through their angles

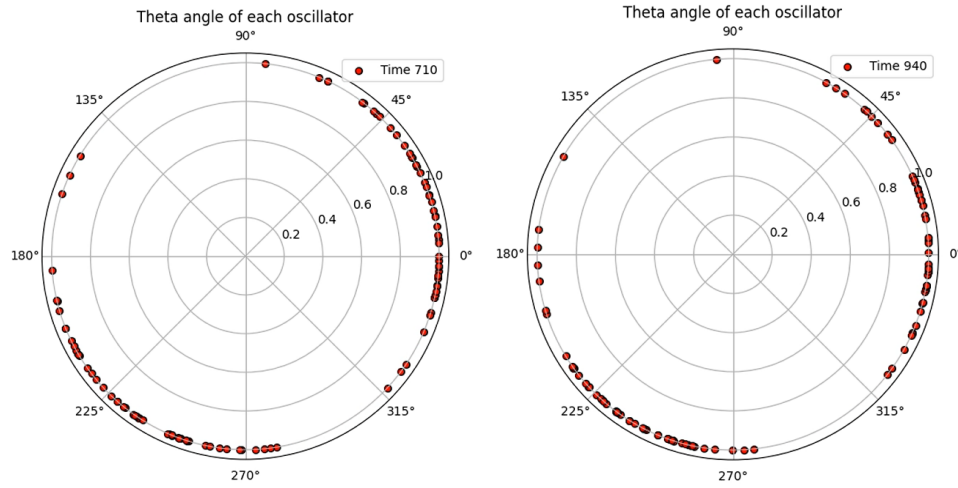


Figure 12: Bimodal distribution. Angle of each oscillator at time  $t=710$  and  $t=940$  for  $K=5$ . Here two clusters are formed. One with the average intrinsic velocity of -1 and the other with +6. Here both clusters are sufficiently tied to not be broken when the other passes

For certain  $K$  always are certain average intrinsic velocities that give only one cluster, as in figure 13. To change the intrinsic velocities to be more different of the other one makes the clusters formed of each average velocity harder to mix with the other group, for example, for  $K=5$  one cluster is formed for intrinsic average velocities of -1 and 1 (Figure 13) and for the same  $K$  two clusters are formed with average velocities -3 and 3 (Figure 14).

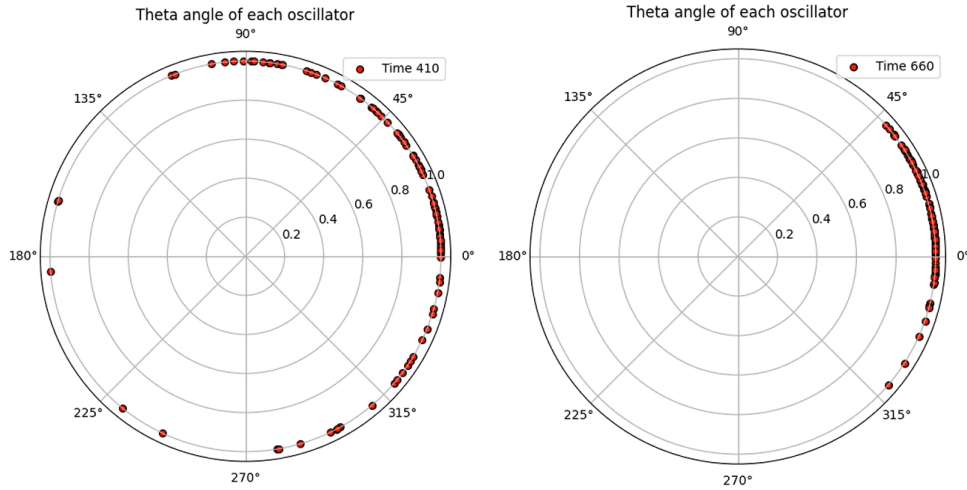


Figure 13: Bimodal distribution. Angle of each oscillator at time  $t=410$  and  $t=660$  for  $K=5$ . Here only one cluster is formed, with around the average velocity of both groups of oscillators, 0 (-1 and +1).

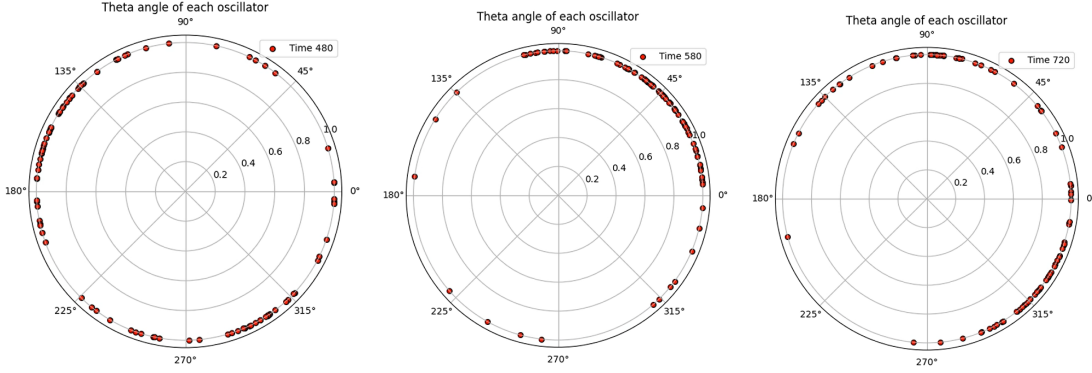


Figure 14: Bimodal distribution. Angle of each oscillator at time  $t=480$ ,  $t=580$  and  $t=940$  for  $K=5$ . Here two clusters are formed. One with the average intrinsic velocity of -3 and the other with +3. Here both clusters are sufficiently tied to not be broken when they cross (as in time  $t=580$ )

If the velocities are sufficiently high and opposite, even with a high  $K$  that makes the two groups unite in a cluster that moves together there is a gap between them. In this case, if  $K$  grows it can be seen that the gap is reduced (Figure 15).

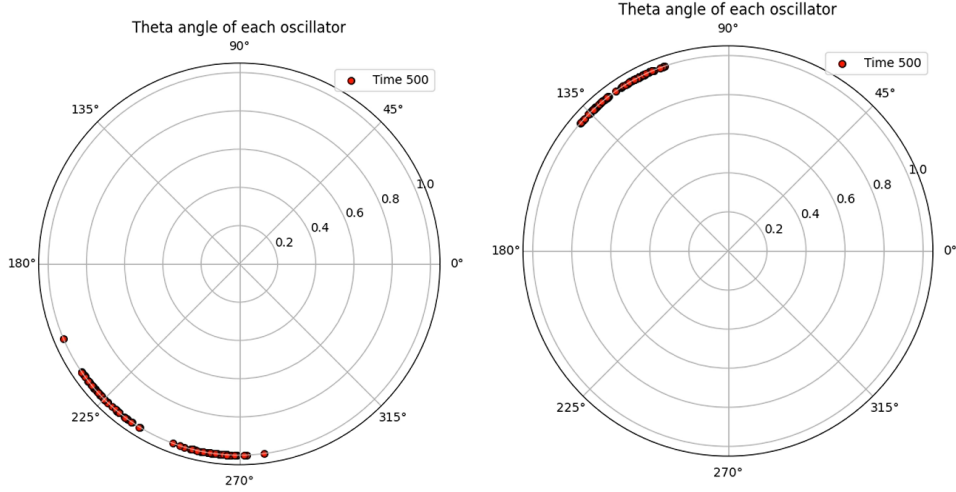


Figure 15: Bimodal distribution. Angle of each oscillator at time  $t=500$  for  $K=10$  and  $K=10$ . Here only one cluster is formed, with around the average velocity of both groups of oscillators, 0 (-3 and +3). It can be seen that as  $K$  are higher the two groups of different intrinsic velocities, now in the same cluster, come closer.

## 5 The Kuramoto's Model in two dimensions. Appearance of patterns associated with Turing instabilities

In 2D, the Kuramoto's model must be different. Contrary to what happens in section 3, here the interaction is no longer between each pair of oscillators, but just with the nearest neighbors (up, down, left, right), as the next equation described:

$$\frac{d\theta_{i,j}}{dt} = \omega_{i,j} + K[\sin(\theta_{i-1,j} - \theta_{i,j}) + \sin(\theta_{i+1,j} - \theta_{i,j}) + \sin(\theta_{i,j-1} - \theta_{i,j}) + \sin(\theta_{i,j+1} - \theta_{i,j})] \quad (5.1)$$

Simulating this type of interaction, with 290x290 oscillators (assuming again that the frequencies obey a lorentzian distribution function with the same properties as in the unimodal case), it was expected that the system creates Turing patterns. In figures 16 it can be seen that Turing patterns (as represented in figure 17) are formed and that  $K$  affects them in the way that the patterns are bigger as bigger is  $K$ .

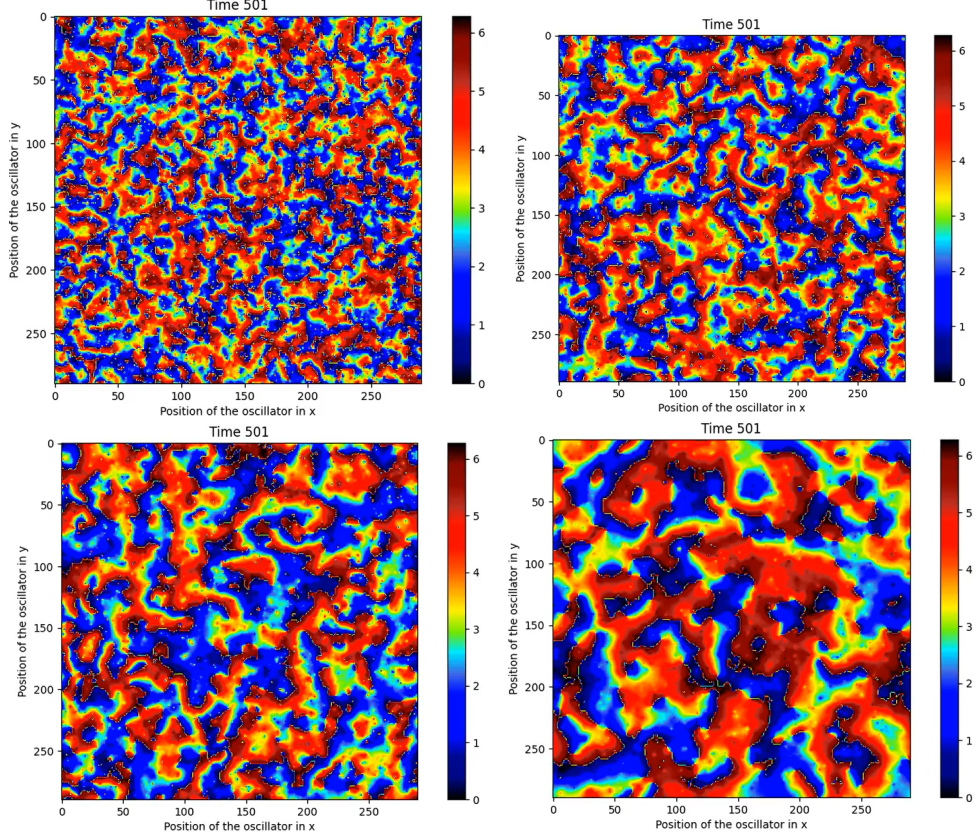


Figure 16: 2D simulation at  $t=501$  for  $K=5$ ,  $K=10$ ,  $K=20$  and  $K=50$  (from top left to bottom right). Each point is an oscillator and the color marks its angle.

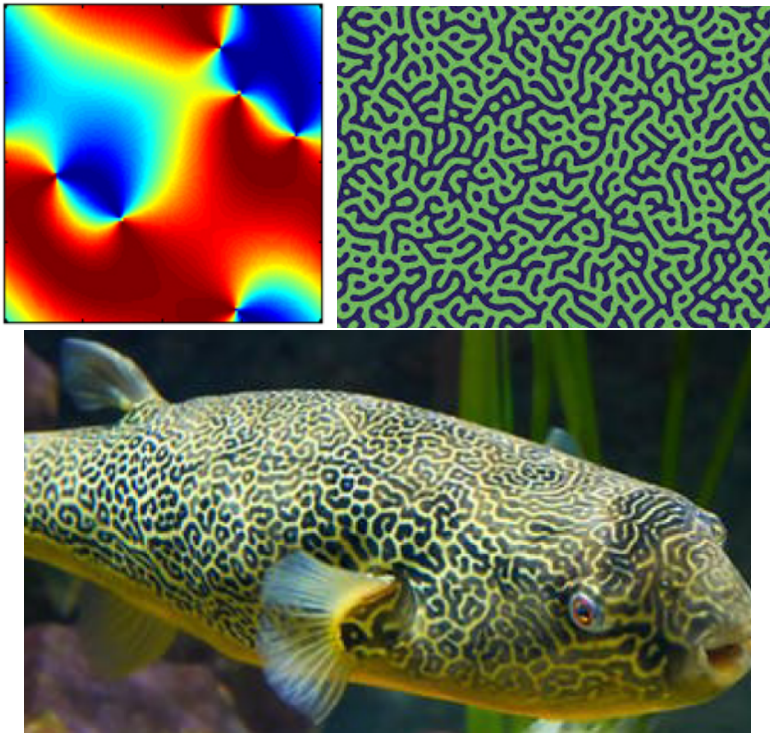


Figure 17: Turing patterns (up)(top left is very similar to the results achieved) and Turing pattern in nature (bottom)

Different types of interactions were tried and similar results were obtained. The other type of interaction varying slightly this type were interactions only with the diagonals, which not proved to give a swirl pattern, but nothing interesting, and nearest neighbour, counting diagonals too, which gave similar results to without counting diagonals.

To investigate deeper, there were extracted simultaneously the angles and velocities of two simulations, one with nearest neighbour and the other with nearest neighbour plus diagonals. For both it was used  $K=50$ , which have the patterns more marked. The angles can be seen in figure 18 and 20 and the velocities in figure 19 and 19.

It can be seen that coupling is stronger in the case that also takes into account the diagonals, as with it each oscillator is coupled with 8 other oscillators instead of 4, doubling the effect of the coupling. This makes the Turing pattern to be even bigger than in the case of only up-down-left-right.

With respect to the velocities, it can be seen that initially they follow a lorentzian distribution, with high values, and they start slowing down, with some noticeable exceptions, which are the vortex that can be seen in the figures. Those are oscillators with a intrinsic velocity so high that overcome the coupling. Those vortex are the main reason of perturbations in theta when  $t$  is high.

As time passes and velocity decreases in absolute value (coupling makes the matrix of oscillators to tend to the average intrinsic velocity: 0), is visible that some oscillators with high intrinsic velocity end up being coupled, while the oscillators with the highest intrinsic velocity keep perturbing the matrix.

It is interesting too that vortex in coupling of nearest neighbours plus diagonals are bigger. This may be because the influence of the oscillator with high intrinsic velocity now influences more oscillators directly. This also explains why there are less vortex in the case with diagonals too, as there the oscillator must overcome the influence os 8 oscillators instead of 4.

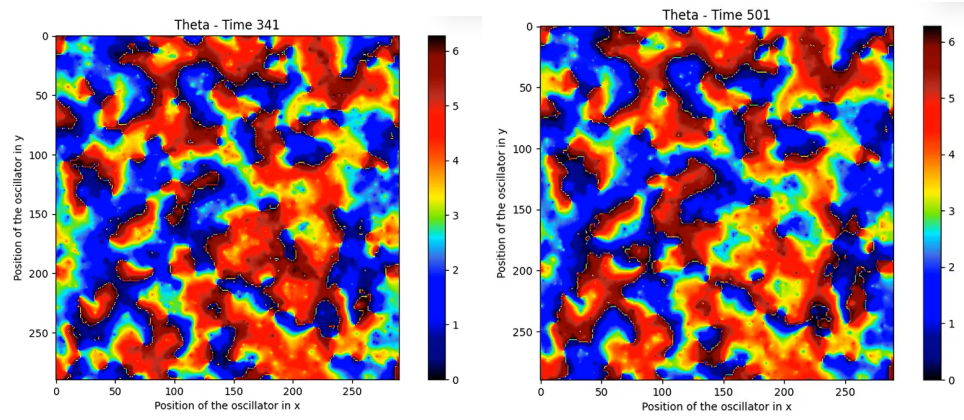


Figure 18: Angles for nearest neighbour,  $K=50$  and time=341 and  $t=501$

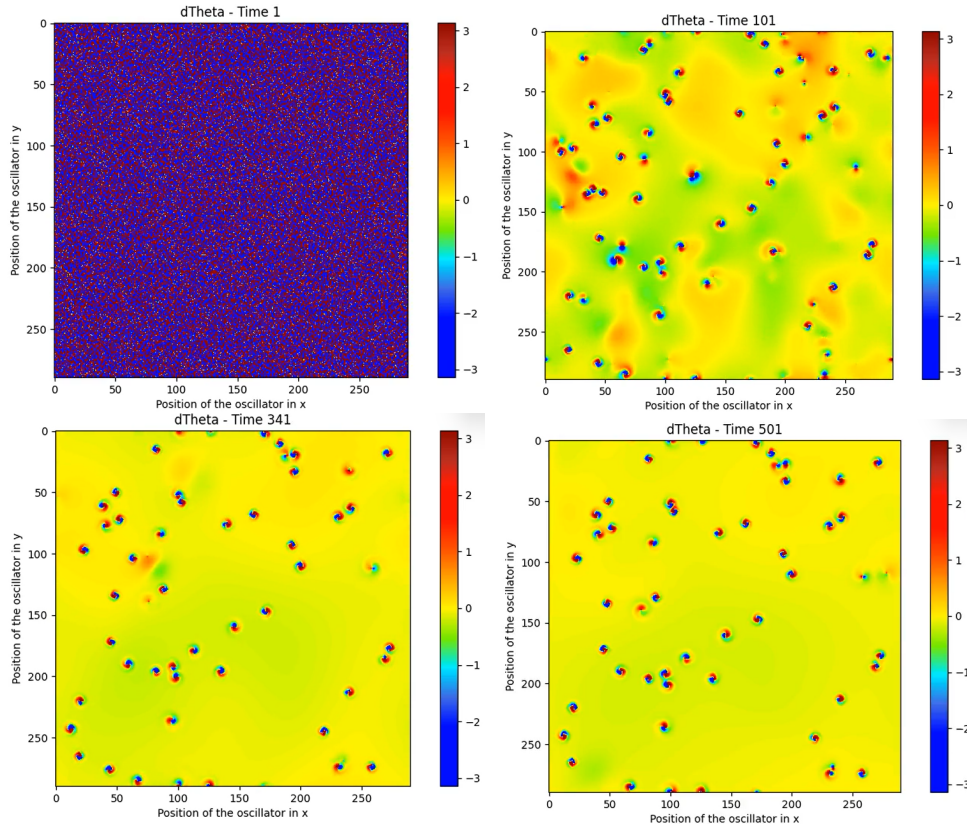


Figure 19: Velocities for nearest neighbour,  $K=50$  and  $t=1$ ,  $t=101$ ,  $t=341$  and  $t=501$

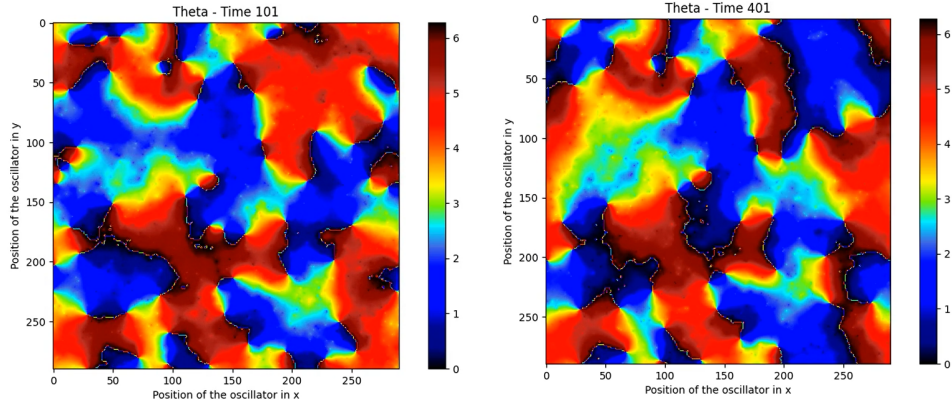


Figure 20: Angles for nearest neighbour plus diagonals,  $K=50$  and time=341 and  $t=501$

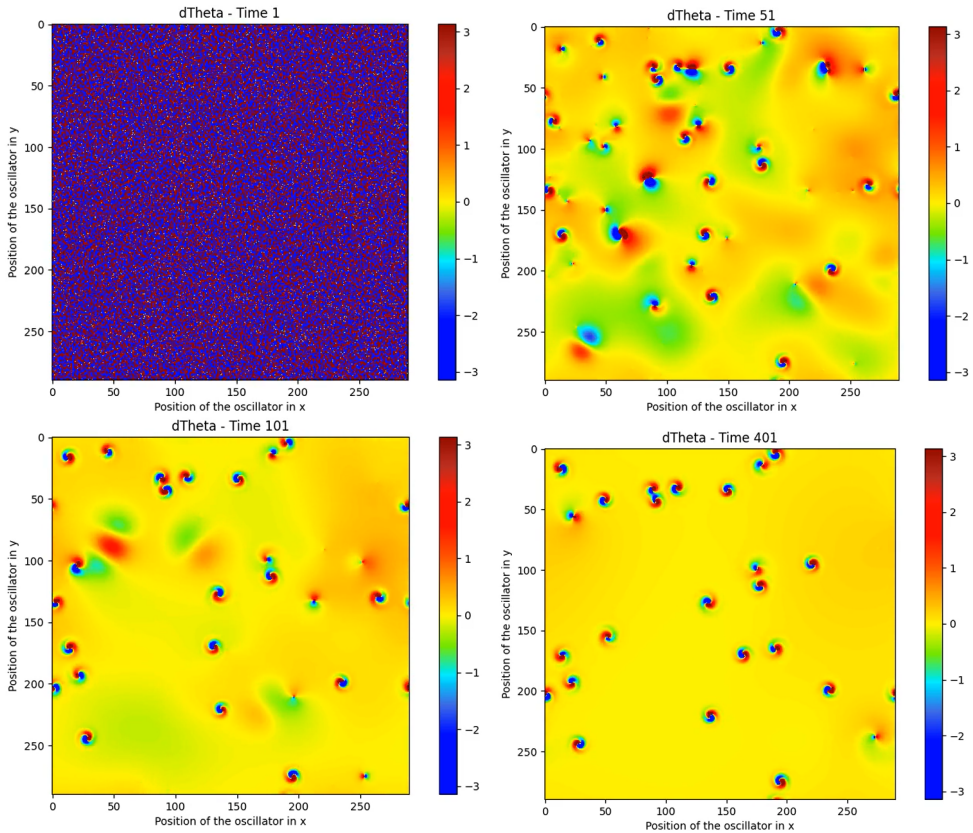


Figure 21: Velocities for nearest neighbour plus diagonals,  $K=50$  and  $t=1$ ,  $t=51$ ,  $t=341$  and  $t=501$

For a better comprehension, all the videos, from which the figures to the previous sections, 3,4 and 5, belong, can be found in the appendix (section 8.2)

## 6 Renormalization Group Analysis of Kuramoto's Model

To end this project, a brief approaching to how renormalize the Kuramoto's model in one dimension (based on what can be seen in [3], [4]).

The Kuramoto model for  $N$  phase oscillators with nearest-neighbor coupling is described by:

$$\dot{\theta}_i = \omega_i + K \sum_{j \in \text{NN}(i)} \sin(\theta_j - \theta_i) \quad (6.1)$$

A position space renormalization by grouping oscillators into blocks would be done as it follows. Each block contains  $L$  oscillators, and we average the phases within each block to form a new effective oscillator:

$$\tilde{\theta}_k = \frac{1}{L} \sum_{i \in \text{block } k} \theta_i \quad (6.2)$$

Then, the new effective frequencies and coupling constants for the blocks are defined.

Removing oscillators with large natural frequencies that do not synchronize with their neighbors: If  $|\omega_i - \omega_j| \gg K$ , the oscillator  $i$  is considered fast and its effects are averaged out.

Then Combining strongly coupled oscillators into a single effective oscillator. If  $K_{ij}$  is large compared to the frequency difference  $|\omega_i - \omega_j|$ , combine  $i$  and  $j$ :

$$\Omega = \frac{K_i \omega_i + K_j \omega_j}{K_i + K_j} \quad (6.3)$$

After that, an adjust with the coupling to neighbors accordingly must be done. Rescaling time and coupling constants the maintaining of the form of the equations is assured. For a block of size  $L$  in 1D:

$$\tilde{\omega}_k \sim \frac{1}{L} \sum_{i=1}^L \omega_i \quad (6.4)$$

$$\tilde{K}_{\text{eff}} \sim \frac{K}{L} \quad (6.5)$$

Finally, the adjust these scalings iteratively to account for larger block sizes ends the process.

Repeat the decimation and renormalization steps until the system's behavior converges to a fixed point or the system size becomes manageable. Analyze the fixed point to determine the system's macroscopic synchronization properties, such as the correlation length and critical coupling strength.

By following these steps, the Kuramoto model can be effectively renormalized in one dimension, providing insights into the critical behavior and synchronization properties of the system.

## 7 Conclusions

In this project we have studied the Kuramoto's model in it's version that is possible to study analytically and we have done it, checking the results with the numerical simulations. It was observed that the theoretical values were in line with the numerical ones successfully with an 1.95% error.

After that, it was studied how the system behaved if there was a bimodal distribution of intrinsic velocities and the results were that in the bimodal case there were many possible outcomes, being a much more susceptible to initial conditions system than the one with only one distribution.

The Kuramoto's model was also studied in 2D, with it's respective change in the equations to adapt the coupling to nearest neighbours and there were seen Turing patterns. Furthermore, it was observed

the case were diagonals were also taken into account and it was observed how the velocities behaved and how they influenced the system at high values of time, as well as how the vortex influenced the system and were influenced by the coupling conditions, if taking into account diagonals or not.

To finish the project and in complement to strengthen what has been in class, a very superficial renormalization analysis about the model has been done, specifying another way to treat the problem and arrive to the same conclusions that has been achieved by the mean field analysis. This part was much less rigorous due to the fact that the attention has been centered in the alternative proposal, but sufficient to understand and focus the problem by this way.

## 8 Appendix

### 8.1 Normalization conditions for the mean field analysis section.

$$\int_{-\pi}^{\pi} \rho(\theta, , t) d\theta = 1$$

$$\int_{-\infty}^{\infty} g(\omega) d\omega = 1$$

### 8.2 Links to the videos, data generated and used for each case and the codes.

Link to the videos related to the section 3:

<https://consigna.ugr.es/?s=download&token=34784981-a6c9-4581-abef-cefdd7af16c>

Link to the videos related to the section 4:

<https://consigna.ugr.es/?s=download&token=5dfce3ef-16b1-47d5-81c8-4a207844be2e>

Values for  $\chi_{th}^2$  (section 4) can be found at:

<https://www.medwave.cl/series/MBE04/5266.html>

Link to the videos related to the section 5:

<https://consigna.ugr.es/?s=download&token=11106f34-32fd-4be4-8016-0aca997fe6f3>

Link to the programs created to do this project:

<https://consigna.ugr.es/?s=download&token=c12ec1f5-41e9-46f2-a1bc-c8e645c452d1>

### 8.3 Errors determination

Error bars shown in figures 9, 10 are calculated as it follows:

Indirect uncertainty treatment for  $y = \frac{1}{1-r^2}$ :

$$\frac{\partial y}{\partial r} = \frac{2r}{(1-r^2)^2} \rightarrow U(x) = \frac{2r}{(1-r^2)^2} U(r)$$

$U(r)$  is calculated directly with the random component  $U_a(r) = \frac{\sigma}{\sqrt{N}}$ ; N=20 samples; t of Student for 20 samples: 1.7247.  $U(r) = U_a(r) * t$

## References

- [1] Juan A. Acebrón. “The Kuramoto model: A simple paradigm for synchronization phenomena”. In: *Reviews of Modern Physics* 77.137 (2005), pp. 139–141. URL: <https://journals.aps.org/rmp/abstract/10.1103/RevModPhys.77.137>.
- [2] Jen God. *Riemann–Lebesgue lemma*. URL: [https://en.wikipedia.org/wiki/Riemann%E2%80%93Lebesgue\\_lemma](https://en.wikipedia.org/wiki/Riemann%E2%80%93Lebesgue_lemma). (accessed: 01.06.2024).
- [3] Oleg Kogan; Jeffrey L. ; Rogers M. ; C. Cross ; G. Refael. “Renormalization Group Approach to Oscillator Synchronization”. In: *Physical Review E* 80.3 (2009), pp. 1–7. URL: <https://journals.aps.org/pre/abstract/10.1103/PhysRevE.80.036206>.
- [4] Hengyun Zhou. *Renormalization Group Analysis of Kuramotos Model*. URL: <https://web.mit.edu/8.334/www/grades/projects/projects15/ZhouHengyun.pdf>. (accessed: 03.06.2024).